Chem

CellPress

Article

# Metal-macrocyclic framework featuring adaptive cavity for precise palladium recognition

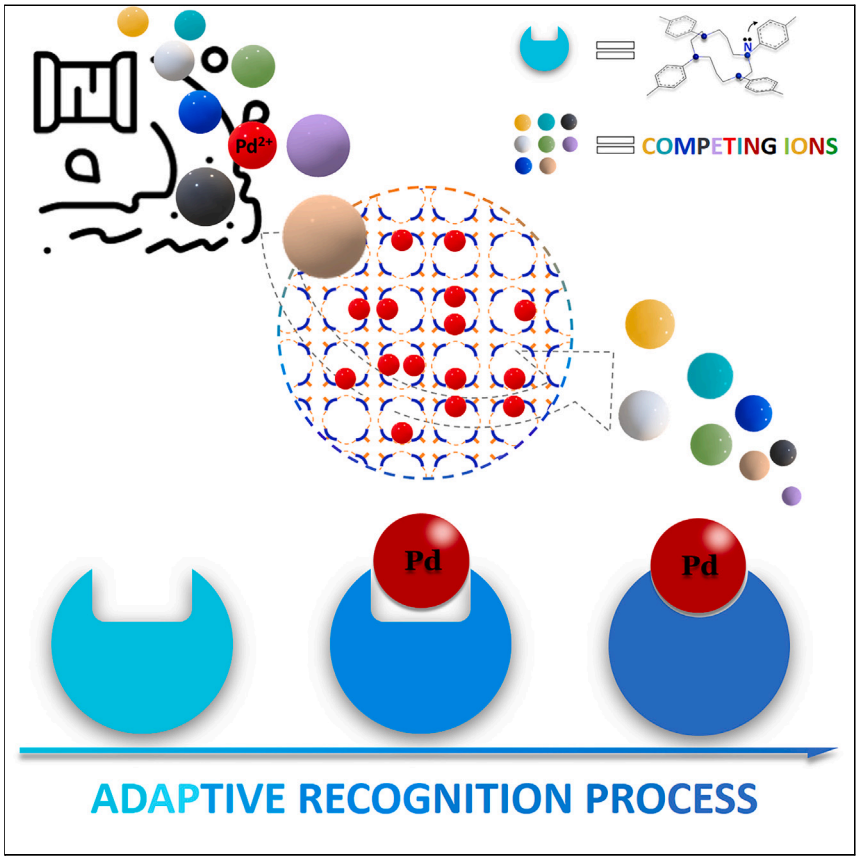


Inspired by how nature uses proteins to recognize and bind specific molecules, this work reports a sorbent material that incorporate special linkers that mimic these natural processes. This new sorbent can adjust itself to trap and hold onto specific substances, such as palladium—a widely used precious metal—from waste. This approach not only captures palladium efficiently but also does so rapidly and selectively, offering a promising way for recovering palladium from diluted sources.

Junyu Ren, Yingxiang Ye, Yin Zhang, ..., Juejing Liu, Xiaofeng Guo, Shengqian Ma

shengqian.ma@unt.edu

## Highlights

This work suggests a new approach for proteomimetics in framework materials

Semi-rigid compounds demonstrate unique chemical properties

The Pd ion is captured efficiently through an adaptive host-guest chemistry process

High selectivity is due to the matchable softness and spatial geometry of N donors

Ren et al., Chem 10, 2776–2791
September 12, 2024 
https://doi.org/10.1016/j.chempr.2024.04.016

CellPress

Chem

Article

# Metal-macrocyclic framework featuring adaptive cavity for precise palladium recognition

Junyu Ren,[1] Yingxiang Ye,[7] Yin Zhang,[1] Weijie Zhang,[4] Qingzhi Liu,[3] Xianqiang Huang,[2] Abdullah M. Al-Enizi,[5] Ayman Nafady,[5] Juejing Liu,[6] Xiaofeng Guo,[6] and Shengqian Ma[1,8,*]

## SUMMARY

**The rational synthesis of advanced porous materials with performances mimicking those of biological proteins remains challenging. Evidently, metal-organic frameworks with dense, rigid aromatic motifs hinder the creation of adaptable cavities with superior guest-to-framework interactions. Herein, a zirconium macrocyclic framework, named metal-macrocyclic framework (MMCF)-6, featuring an adaptive cavity, was constructed using a cyclam-based linker. The vacant yet adaptable cyclam cavity in MMCF-6 renders it capable of precisely recognizing $Pd^{2+}$ in aqueous solution with a high uptake capacity of 326 mg $g^{-1}$ and extraordinary recovery efficiency of >99.99%. The characteristic proteomimetic behavior of MMCF-6, that is, guest-induced fit during the $Pd^{2+}$ recovery, was unveiled by combined studies of X-ray crystallography, extended X-ray absorption fine structure, and density functional theory, which provided unambiguous confirmation of the cyclam macrocycle's allosteric behavior accountable for the excellent Pd capture performance. Our work herein opens a new avenue by incorporating semi-rigid cavities into framework materials for efficient host-guest chemistry.**

## INTRODUCTION

Insights on how to achieve a semi-rigid state, in which donors are kept in the near ideal position by α/β folds or hydrogen bonds with certain degree of local structural flexibility, can be learned from nature's protein recognition event.[1] Subtle local environment fluctuations on the active-site, which are often fundamentally related to proteins' interacting mechanisms with guests, have been magnified and demonstrated to significantly alter the essential protein properties.[2,3] Similar to enzymes, local environmental changes stimulated by guest molecules intruding into the porous skeletons are greatly desired in artificial hosts, leading to dynamic optimization of the host-guest chemistry related to the structural or other desired responses toward targets and thus could differentiate them from traditional materials.[4,5] Although the aforementioned adaptive alteration of pore environment is a remarkable characteristic, successful design and systematic studies have been seldomly reported.

As a member of the platinum group metal (PGM), palladium (Pd) exhibits a variety of unusual physical, chemical, and mechanical properties.[6,7] Pd's growing demand in industry, along with its rarity from terrestrial ores, necessitates a secondary source. The recovery of PGMs from wasted processes is a potential alternative for reducing reliance on a limited source.[8–10] The concentration of Pd and its competing ions may

## THE BIGGER PICTURE

Nature's protein recognition mechanisms provide a blueprint for creating ideal sorbents, which are achievable in metal-organic frameworks (MOFs). By incorporating macrocyclic linkers, MOFs can create dynamic environments that facilitate guest molecule interactions, similar to biological functions. These macrocycles play a crucial role in regulating guest movement and recognition, leading to proteomimetic sorbents. Herein, we report a zirconium-based MOF bearing *in-situ*-generated semi-rigid binding pockets for $Pd^{2+}$ featuring high uptake capacity, fast kinetics, and stability under acidic conditions with high selectivity. This approach leads to the creation of novel aza-macrocycle-binding pockets, enabling efficient one-round enrichment and purification of palladium from simulated waste solutions. Therefore, this strategy paves the way for developing adaptable sorbents with dramatically enhanced uptake capacity and selectivity.

 

vary across different scenarios, making it essential to have a sorbent with high selectivity that can target Pd while excluding other ions (Tables S5–S8).[11] In solvent extraction techniques, it shows how multidentate ligands improve Pd uptake. Benefiting from the fact that the donors are linked by alkyl chains, which allow for certain degree of rotational mobility, extractants such as malonamides, diglycolamides, and carbamoyl methylphosphine oxides have been widely applied for the Pd recovery.[12,13] Although open-chain extractants maximize the number of donors that may chelate metal ions, the tendency of redundant ligand coordination diminishes the metal selectivity. As learned from the protein complexation process, in which adaptable donors are organized in a specified order to maximize binding affinity and selectivity, bonding mobile donors in a certain spatial layout inside the sorbents is promising for achieving metal binding preference (Figure 1A).[1] Taking advantage of the cave-like donor geometries, macrocycles are one of those ligands that are intensely used as chelator/receptors in coordination and supramolecular chemistry.[14–19] One of the most-studied macrocycle-based materials is that based on crown ethers, which is reported for applications in molecular recognition, hydrogen storage, pollution remediation, and enantioseparation.[20–23] However, based on the hard and soft acid and base (HSAB) theory, the affinity between Pd (soft acid) and the oxygen species (hard base) is moderate.[24] Furthermore, from a chemical standpoint, researchers have limited methods for modulating the chemical nature of oxygen species, owing to the inherent restriction that oxygen usually forms covalent bonds with two adjacent atoms. Aza-macrocycles (or aza-crown ethers) are nitrogen (N)-analogs of crown ether. Cyclam, a 14-membered aza-macrocycle that exists in a "transition region" between giant aza-crown ethers and small aza-rings, shows moderate conformational flexibility while possessing a relatively large cavity suitable for host-guest chemistry.[14,25–27] Compared with other analogs of the aza-macrocycle family, such as TACN (1,4,7-Triazacyclononane, 9-membered) and cyclen (12-membered), cyclam-based sorbents hold promise to be applied in Pd-recovery, especially considering the following: (1) cyclam guarantees a preferred geometry of the N-donors by holding them with an optimal N–N distance for potential cooperation and hence improves the global order of donors in the built adsorbents, (2) the mobile nature of the alkyl constituents enables adaptive host-guest chemistry, during which the local conformation of cyclam keeps rearranging until final chelation, and (3) ion affinity of the aza-cavity could be adjusted across a wide range depending on the chemical environment in which the N is connected.[28–30] Taking advantage of the above, cyclam systems can potentially make more efficient contact with $Pd^{2+}$ compared with TACN/cyclen or rigid compounds while being more selective compared with the open-chain extractants. Nonetheless, neither any rational design nor function-led synthesis, which enables cyclam-based sorbents with guest-accessible cavities and a molecular-level predesign of local dynamics, has been proposed so far (Table 1).

Metal-organic frameworks (MOFs) are a well-known family of crystalline porous materials with fascinating structures and intriguing properties.[34–36] Designing and incorporating linkers with local motions is integral in developing novel MOF sorbents.[4,37,38] Macrocyclic linkers bring well-tailored local environments (often with allosteric nature), which play an important role in regulating guest traffic in channels and guest recognition/uptake.[39–42] With the functionalization on amino sites and metalation, cyclam could be integrated into a broader variety of compounds compared with its O analogs through different topologies.[14,25,28,30] Nonetheless, for the identified cyclam-based MOFs, either a labile framework or blocked macrocycles has been shown, hence precluding studies on the macrocyclic host.[31,33,43–45] Given the significant role of aza-macrocycle, a deliberate design is necessary to

[1]Department of Chemistry, University of North Texas, 1508 W Mulberry St, Denton, TX 76201, USA

[2]Shandong Provincial Key Laboratory of Chemical Energy Storage and Novel Cell Technology, School of Chemistry & Chemical Engineering, Liaocheng University, Liaocheng 252059, Shandong, China

[3]College of Chemistry and Pharmaceutical Science, Qingdao Agriculture University, No. 700 Changcheng Road, Qingdao 266109, China

[4]Department of Chemistry, University of Virginia, Charlottesville, VA 22904, USA

[5]Department of Chemistry, College of Science, King Saud University, Riyadh 11451, Saudi Arabia

[6]Department of Chemistry, Washington State University, Pullman, WA 99164, USA

[7]Fujian Provincial Key Laboratory of Polymer Materials, College of Chemistry and Materials Science, Fujian Normal University, Fuzhou 350117, Fujian, China

[8]Lead contact

*Correspondence: shengqian.ma@unt.edu

https://doi.org/10.1016/j.chempr.2024.04.016

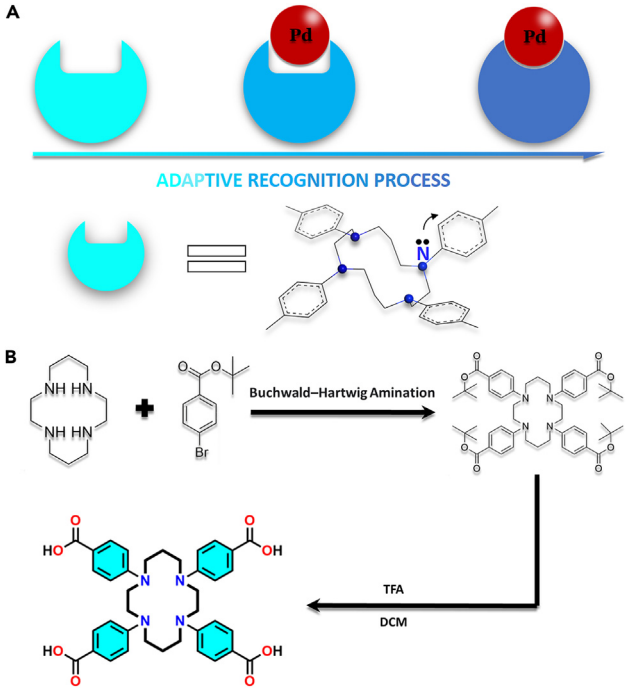


**Figure 1. Schematic representations of the adaptive recognition process and the linker synthesis route**

(A) Adaptive $Pd^{2+}$ recovery process.

(B) Synthesis of **$H_4$L** (4,4′,4″,4‴-(1,4,8,11-tetraazacyclotetradecane-1,4,8,11-tetrayl)tetrabenzoic acid).

strike a balance between its adaptability and the framework robustness. With the customizable feature of MOFs, one may anticipate the existence of a cyclam compound-SBU (SBU: secondary building unit) combination, exhibiting both a robust skeleton and an open cavity that can be used for Pd recovery.

Herein, by direct arylation of the cyclam macrocycle via the Buchwald-Hartwig amination, together with the participation of Zr-carboxylate moieties, we report a new porous cyclam-based zirconium MOF, $[Zr_6(\mu_3\text{-}OH)_4(OH)_4(L)_3]$ (L = 4,4′,4″4‴-(1,4,8,11-tetraazacyclotetradecane-1,4,8,11-tetrayl)tetrabenzoate), which is denoted as MMCF-6 (MMCF = metal-macrocyclic framework) featuring accessible

**Table 1. Representative MOFs based on cyclam**

| Compound | Surface area ($m^2\ g^{-1}$) | Ligand's rigidity | Metalation | Accessibility of the macrocycle |
|---|---|---|---|---|
| $[Ni(cyclam)(bpydc)]\cdot 5H_2O$[a] | 817 | rigid | Ni | no |
| $[Ni(cyclam)]_2[BPTC]_n\cdot 2nH_2O$[b] | – | rigid | Ni | no |
| $[Ln(H_2TETA)]NO_3\cdot 2H_2O$[c] | – | flexible | no | no |
| VPI-100 (Cu, Ni)[d] | 398/612 | rigid | Cu, Ni | no |
| MMCF-6[e] | 1,300 | semi-rigid | no | yes |

[a]bpydc = 2,2′-bipyridyl-5,5′-dicarboxylate.[31]

[b]BPTC = 1,1′-biphenyl-2,2′,6,6′-tetracarboxylate.[32]

[c]$H_2$TETA = 1,4,8,11-tetraazacyclotetradecane-1,4,8,11-tetraacetic acid.[33]

[d]VPI-100 (Cu) and VPI-100 (Ni) (VPI, Virginia Polytechnic Institute). $[Zr_6(\mu_3OH)_8(OH)_8(M\text{-}L)_4]$, where M = Cu(II) or Ni(II), L = 6,13-dicarboxy-1,4,8,11-tetraazacyclotetradecane).[43]

[e]This work.

cyclam cavities. MMCF-6 differs from other macrocyclic frameworks in that it does not necessitate metalation to maintain the geometry of cyclam macrocycle, which allows for guests to readily interact with the cyclam cavity, while it still retains permanent porosity as confirmed by $N_2$ sorption isotherms measurement. These features bestow MMCF-6 with excellent capability in extracting $Pd^{2+}$ from an aqueous solution with a high adsorption capacity of 326 mg $g^{-1}$, as well as rapid kinetics of recovering >99.9% Pd within 5 min and an extraordinary recovery efficiency of >99.99% after 3 h. The affinity between the soft Lewis acid and base induces the relocation of N donors, thereby realizing adaptive host-guest chemistry, and leads to a high uptake capability and fast kinetics. This was clearly confirmed by the combined studies of X-ray crystallography, extended X-ray absorption fine structure (EXAFS), and density functional theory (DFT) calculations. This research work establishes a paradigm for the construction of macrocyclic frameworks with open cavities and acts as a springboard for further development of this family of materials in applications of PGM recovery and beyond.

## RESULTS AND DISCUSSION

### Synthesis, structural characterization, and porosity analysis of MMCF-6

To construct a cyclam-based MOF for efficient Pd recovery, one should consider rationally designing macrocyclic ligands to meet the following criteria: (1) the intramolecular freedom should be minimized, which could contribute to framework robustness,[33,43–46] (2) the as-synthesized MOF should maintain the accessibility of the cyclam macrocycle, which necessitates the elimination of the metal core and the preservation of a coplanarity geometry, (3) Pd affinity should be attained by chemical environment customization, and (4) facile synthesis should be performed because it is necessary for possible practical application. We envision that the direct arylation on amines could suppress the intramolecular freedom, allowing for the ordered self-assembly and sustaining of the aza-macrocycle framework without metalation. Furthermore, the amine's basicity could be tuned via the conjugation effect to a "softer" base that, in accordance with the HSAB theory, tends to bond with the soft acid $Pd^{2+}$.[24] The aforementioned criteria were met by a newly designed ligand, 4,4′,4″,4‴-(1,4,8,11-tetraazacyclotetradecane-1,4,8,11-tetrayl)tetrabenzoic acid ($H_4L$), which was easily prepared through one step of C–N cross-coupling and subsequent hydrolysis in acidic environments (Figures 1B and S1). Considering the steric effect, the secondary amines in aza-macrocycles are regarded as challenging substrates for Pd-catalyzed arylation; in this work, it was overcome by carefully selecting Buchwald-Hartwig amination conditions.[47–50]

MMCF-6 was synthesized by the solvothermal reaction of $ZrCl_4$ and $H_4L$ in N,N′-dimethylformamide (DMF) at 100°C for 24 h with the presence of acetic acid as modulator (Figure S2). The crystal structure of MMCF-6 was analyzed by single-crystal X-ray diffraction (SCXRD) combined with Rietveld refinement on experimental powder X-ray diffraction (PXRD) pattern. SCXRD revealed that MMCF-6 crystallizes in the *Pm-3m* space group with an *ftw* topology, as MOF-525/PCN-221 previously demonstrated (Figures 2A and S3; Table S1). MMCF-6 has a cubic structure comprising twelve connected $Zr_6$-oxo clusters and the four connected tetra-topic L linker with a pore diameter of ~15 Å, and a formula of $[Zr_6O_4(OH)_4(L)_3]$•(solv)x, where solv is the solvent molecule. Rietveld refinement on the PXRD patterns further confirmed the phase purity of the obtained material (Figures S8 and S9; Table S2). Typically, these alkyl-based macrocycles possess extensive conformational possibilities accessible through manifold low-energy-barrier torsions. Cyclam and other fourteen-membered tetra-aza-macrocycles are

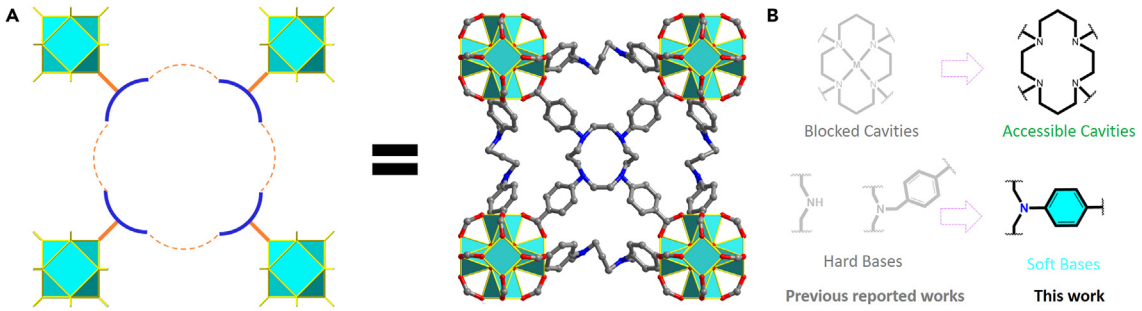


**Figure 2. Crystal structures and design concept of MMCF-6**

(A) MMCF-6 crystalizes in a *ftw* topology. Pore structure viewed along the c axis showing cubic cage.

(B) Comparison of previous reported cyclam-based MOFs with the one in this work.

moderately flexible structures and can exhibit in both *trans* (nearly coplanar) and *cis* geometries when coordinated. Here, based on the X-ray crystallography studies and DFT calculations, cyclam with a *trans*-planar geometry is dominant in MMCF-6 and thus with **L** approaching to a coplanar geometry. Additionally, SCXRD tests reveal a conformational difference between the free esterified ligand (**compound 3**) and its integration into MMCF-6 (see Figures S4–S6; Table S3). Constructing a plane across the four N atoms within cyclam shows variation in the orientation of the benzoate moieties: in **compound 3**, two tert-butyl benzoates form a 15° angle with the plane, whereas the other two exhibit a 60° angle; in **L**, two benzoates are positioned at a 30° angle to the plane, with the remaining two at a 40° angle. This observation underscores the semi-rigid nature of **L**, distinguishing it from other MOF ligands that possess a rigid structure, and affords it unique sorption behaviors for targeting guest molecules. The transformation can be elucidated as follows: the growth of MOF crystals is a dynamic process where the linkers bridge between metal clusters; the conformation of these linkers transforms due to elevated temperatures, coordination with the Zr cluster, and integration into the framework, contributing to the observed conformational differences.

Following the removal of the guest molecules, $N_2$ sorption isotherms at 77 K were measured to assess MMCF-6's permanent porosity, which shows a type-I profile with a Brunauer-Emmett-Teller (BET) surface area of 1,300 $m^2\ g^{-1}$ (Figure S14). The total pore volume of MMCF-6 as determined by the single-point method is 0.65 $cm^3\ g^{-1}$. The pore size distribution calculated by non-local DFT (NL-DFT) from the $N_2$ sorption curve indicates that the pores of MMCF-6 are predominantly distributed at ca. 13.1 Å, which are consistent with the pore size observed from crystal structure when the van der Waals contact is considered. The hysteresis loop is likely caused by gradual desorption process, which is frequently seen in sorbents with different size pores being combined.[51]

According to the results of the thermogravimetric measurement, MMCF-6 can be stable up to 573 K under a $N_2$ environment (Figure S10). Although MMCF-6 comprises a ligand based on a flexible macrocycle, it still exhibits significant chemical stability in a wide variety of solvents and aqueous solutions over a broad pH range (Figures S15 and S16). Following 7 days of immersion in water and aqueous solutions with a pH range from 2 to 10, $N_2$ sorption isotherms of MMCF-6 (Figure S17) are comparable to that of the pristine sample, highlighting its framework robustness and structural stability. The morphology for the MMCF-6 sample was revealed by scanning electron microscopy (SEM) measurements as homogeneous cubic-shaped crystals (Figures S11 and S12).

### Assessment of Pd capture by MMCF-6

Based on the HSAB theory, hard acids prefer binding to the hard bases (generating bonding with ionic nature), whereas the soft acids prefer binding to the soft bases (generating bonding with covalent nature).[24] $Pd^{2+}$ is a soft acid, thereby preferring formation of covalent complexes with soft base. With the direct bonding with the benzene ring, the N atoms in L were modified to a "softer" base because of delocalization of the lone pair at N (Figure 2B). We envision that the open cyclam cavity, preorganized N donor geometries, and compatible Lewis basicity will enable an efficient chelation toward $Pd^{2+}$, which contributes to interactions with Pd and thus enable effective and efficient recovery behavior.

To obtain Pd adsorption isotherms, solutions of increasing $Pd^{2+}$ concentrations (25–800 ppm) were treated with the adsorbents. The solution was stirred for 24 h until the equilibrium concentration was reached, which was then filtered and analyzed via inductively coupled plasma optical emission spectrometry (ICP-OES) to determine the residual $Pd^{2+}$ concentration. From the isotherms (Figure 3A), MMCF-6's adsorption behavior can be fit with the Langmuir model and shows a saturation uptake capacity of 326 mg $g^{-1}$ at the equilibrium concentration of 426 ppm.

With the promising results from Pd extraction, the kinetics and recovery efficiency of MMCF-6 toward $Pd^{2+}$ was investigated. With 50 mg of the adsorbent suspended in 500 mL of a 5 ppm $Pd^{2+}$ solution, the data points were collected from 3 min to 3 h using ICP to measure the remaining $Pd^{2+}$. MMCF-6 was able to rapidly recover >99.9% Pd within 5 min, and after a 3 h period, the residue concentration of $Pd^{2+}$ in solution was 0.23 ppb (Figure 3B), which means that is has an extraordinary recovery efficiency of >99.99%. The kinetic data were fit to a pseudo second-order kinetic model, indicating that the rate-limiting step is a chemisorption process. The distribution coefficient ($K_d$) was used here to assess the adsorption affinity, a crucial property for Pd recovery from dilute wastewater. Based on the kinetic data, the $K_d$ was calculated to be $4.7 \times 10^6$ mL $g^{-1}$ (Figure S18), indicative of strong binding between cyclam cavities and $Pd^{2+}$ ions, which could be ascribed to the presence of highly preorganized binding cavities within MMCF-6. Additionally, as a hierarchically porous material with two levels of pores, i.e., one from the frameworks and the other one from the macrocycles, MMCF-6 allows for efficient mass-transfer and strong capture behavior, which contribute to the rapid $Pd^{2+}$ uptake through the nanoconfinement effect.

Utilizing a dynamic column breakthrough experiment, we then investigated the $Pd^{2+}$ recovery capability of MMCF-6 to confirm its potential for practical usage (Figures 3D and S25). Initially, full $Pd^{2+}$ adsorption from the original 430 mL solution is observed. The decreasing trend of available binding sites then leads to gradual increase of $Pd^{2+}$ concentration in the effluent solution, which continues to increase as the number of available binding sites decreases. After passing through ~1,320 mL of simulated waste solution, the column eventually reaches adsorption equilibrium. The dynamic capacity is close to the static capacity, further highlighting the strong affinity of MMCF-6 for $Pd^{2+}$. To examine the recyclability of MMCF-6, *in situ* flow of 0.05 M thiourea through the Pd-adsorbed column was used to evaluate online desorption behaviors. The desorption ratio was determined to be 93%. To further establish the reusability of MMCF-6, 19 additional adsorption desorption cycles were conducted using dynamic column separation (Figure 3C). MMCF-6's practical usefulness is also demonstrated by the intact PXRD pattern after dynamic adsorption and *in situ* desorption (Figures S26 and S27).

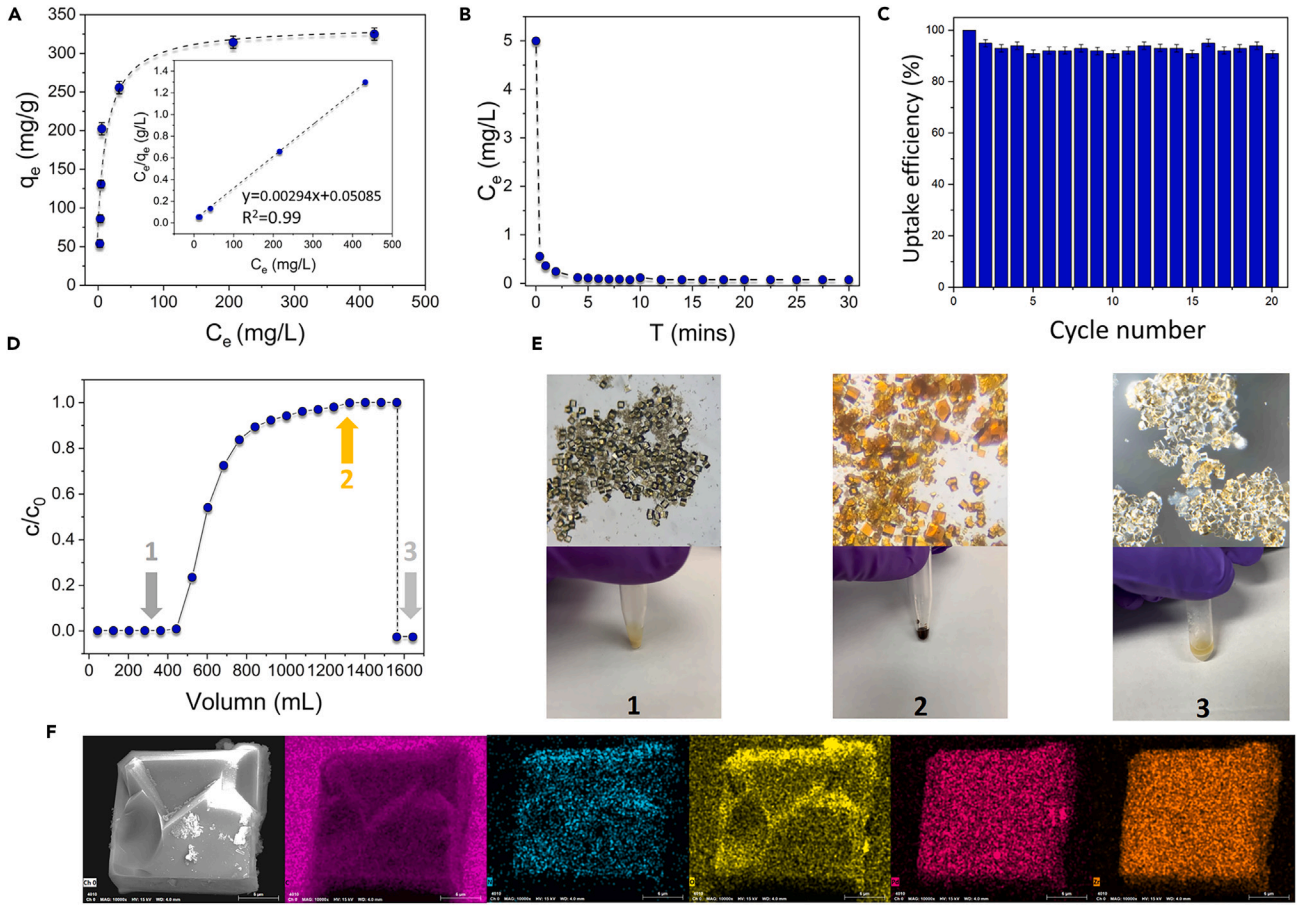


**Figure 3. Results of palladium adsorption experiments**

(A) $Pd^{2+}$ adsorption isotherms (error bars represent standard errors); inset: linear regression fit with the Langmuir model).

(B) $Pd^{2+}$ adsorption kinetics. Fast $Pd^{2+}$ uptake kinetics show the high $Pd^{2+}$ affinity of MMCF-6.

(C) Reusability of MMCF-6 with 20 adsorption-desorption cycles (error bars represent standard errors).

(D) Dynamic adsorption curve of MMCF-6-packed column for $Pd^{2+}$ separation.

(E) Optical micrographs of MMCF-6 crystals before and after Pd uptake and after regeneration by thiourea.

(F) EDS elemental mappings for Pd@MMCF-6 (scale bar: 6 μm).

## Pd ion selectivity

The selectivity of MMCF-6 for $Pd^{2+}$ in the presence of other ions prevalent in waste streams was systematically evaluated. There are several major scenarios containing Pd as an important secondary source, such as waste electrical and electronic equipment (WEEE), electroplating waste water, spent automobile catalyst (SAC), and high-level liquid waste (HLLW).[52–55] The major competing ions in the above cases are listed in Tables S5–S8.

Based on Pearson HSAB theory, those ions could be divided into hard acids, borderline acids, and soft acids (Table S9).[56] However, it should be noted here that all hard/soft acids and bases are not equally hard/soft. There is a graduation in hardness/softness, and there are a number of borderline acids and bases that do not fit neatly in either category. Borderline acids can be considered hard or soft depending on their oxidation state (higher-oxidation-state species can be considered as hard acids and lower-oxidation-state species as soft acids).[56–58]

The selectivity of MMCF-6 toward hard acids was examined by exposing a sample of MMCF-6 to an aqueous solution containing 10 ppm of the $Pd^{2+}$ ion and a number of other competing metal ions ($Na^{+}$, $K^{+}$, $Mg^{2+}$, $Y^{3+}$, $La^{3+}$, $Zr^{4+}$, $V^{3+}$, $Nd^{3+}$, $Fe^{3+}$, $Al^{3+}$, $Cr^{3+}$, and $Hf^{4+}$. See Table S10 for the metal source). Not surprisingly, MMCF-6 exhibited 98% recovery rate for $Pd^{2+}$, which is significantly higher than other ions (others less than 4.5%, Figure S20B). This is due to the mismatch of hardness/softness according to the HSAB theory. For borderline/soft acids ($Fe^{2+}$, $Co^{2+}$, $Ni^{2+}$, $Cu^{2+}$, $Zn^{2+}$, $Pb^{2+}$, $Rh^{3+}$, $Ru^{3+}$, $Ag^{+}$, $Pt^{4+}$, $Cd^{2+}$, and $Hg^{2+}$), separate sorption isotherms were collected and compared (Figures S21–S24). Among those ions, the separation of Pd and platinum (Pt) was particularly challenging, given the similarity of their chemical properties. The Pt uptake of MMCF-6 was 148 mg $g^{-1}$ at 500 mg $L^{-1}$ concentration in the single-ion sorption test. We then conducted a competing sorption experiment in a mixture solution of $Pd^{2+}$, $Pt^{4+}$, $Ru^{3+}$, and $Rh^{3+}$. MMCF-6 was observed to perform optimal selectivity in capturing $Pd^{2+}$ over $Pt^{4+}$, $Ru^{3+}$, and $Rh^{3+}$ when we adjusted the solution to pH = 3 with HCl. The recovery rate of $Pd^{2+}$ is five times that of $Pt^{4+}$ and 18.4 and 46 times that of $Ru^{3+}$ and $Rh^{3+}$, respectively. Under an acidic condition with a high concentration of $Cl^{-}$, $Pt^{4+}$ will form octahedral $[PtCl_6]^{2-}$ with a size of 8.3 Å, whereas Pd presents as $[PdCl_4]^{2-}$ in square planar geometry with a size of 5.5 Å. The enhanced selectivity for Pd can be attributed to the smaller size of $[PdCl_4]^{2-}$, which facilitates faster diffusion through the hierarchical pore network, enabling it to reach the binding cavity more efficiently. Additionally, the smaller size contributes to a stronger nanoconfinement effect within the micropores, further improving the selectivity. In the single-ion sorption experiments, the uptake capacities of $Ru^{3+}$ and $Rh^{3+}$ are 46.8 and 53.6 mg $g^{-1}$, respectively, at a concentration of 500 mg $L^{-1}$. Although Ru and Rh belong to the platinum group and possess similar 3d orbitals to Pd, their ionic affinity for MMCF-6 is relatively weak. This lack of affinity is due to the mismatch in softness between $Ru^{3+}$/$Rh^{3+}$ and MMCF-6, with $Ru^{3+}$ and $Rh^{3+}$ being classified as borderline acids according to the HSAB theory.

UIO-67-bipyridine and MOF-525 were studied as control materials because they have densely distributed N sites. The Pd-uptake capacity was tested to be 91 and 88 mg $g^{-1}$ at a Pd concentration of 500 mg $L^{-1}$ for UIO-67-bipyridine and MOF-525, respectively. The progressive increase of the sorption curve suggest that electrostatic attraction is the predominant mechanism underlying the adsorption process. The selectivity of UIO-67-bipyridine for Pd was relatively low as observed from competing sorption tests (Figure S19B). It is likely due to two primary factors: (1) the inherent stiffness of the bipyridine compound, which requires additional energy to overcome the activation barrier for subsequent coordination and (2) the presence of *cis-trans* isomerism in the ligand, which impedes the immediate chelation with Pd. We further synthesized MOF-525 (or PCN-221), which is an isostructural MOF of MMCF-6 with tetrakis(4-carboxyphenyl)porphyrin (TCPP) as ligand. It shows a Pd-uptake capacity of 88 mg $g^{-1}$ at a Pd concentration of 420 mg $L^{-1}$. Despite possessing densely distributed N sites in their structures, both UIO-67-pyridine and MOF-525 (PCN-221) do not exhibit promising performance in Pd recovery, especially at a Pd concentration below 100 mg/L.

Table S4 summarizes a comparison of the $Pd^{2+}$ adsorption capacity between MMCF-6 and other representative Pd-recovery adsorbents reported in the literature. Among the MOF-based sorbents, MMCF-6 stands out for its high Pd-uptake capacity, rapid sorption kinetics, and high recovery rate of Pd, even in solutions with ultralow concentrations. Pure organic sorbents, such as CITCFs (covalent isothiocyanurate frameworks) and POP-o$NH_2$-Py, demonstrate a high gravimetric

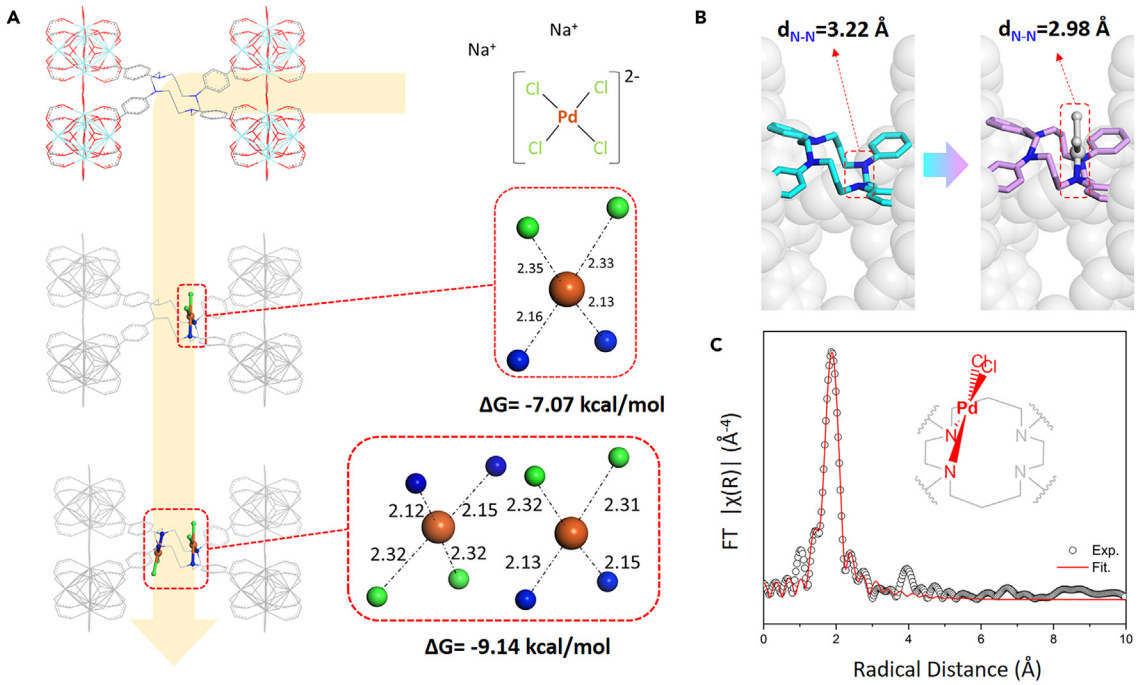


**Figure 4. Results of the Pd adsorption mechanism studies**

(A) The front and local views of two thermodynamically feasible coordination geometry of $Pd^{2+}$ binding with MMCF-6. The number near oxygen or nitrogen atoms is the distance (Å) between the donor atom and $Pd^{2+}$. ΔG denotes the Gibbs free energy changes. Blue, nitrogen; rufous, palladium; green, chlorine.

(B) Comparison of N–N distance before and after $Pd^{2+}$ coordination.

(C) EXAFS fitting of Pd@MMCF-6 (inset: proposed structure of Pd-adsorbed cyclam-cavity).

uptake capacity of Pd, benefiting from their lightweight nature. Composite systems featuring mesoporous structures demonstrate moderate performance, despite their large surface area and favorable pore accessibility. Furthermore, it has been observed that sorbents capable of forming coordinate bonds with $Pd^{2+}$ ions exhibit a stronger affinity for Pd, especially at low concentrations. This finding highlights the importance of aligning the chemical and structural attributes of the sorbents with the specific adsorption needs of Pd ions to enhance recovery efficiency.

## Investigation of Pd adsorption mechanism

To explore the optimal coordination mode of $Pd^{2+}$ in MMCF-6, theoretical models representing the structural features of MMCF-6 were built, as shown in Figure S28. In accordance with the amount of amine-N, the feasible configuration of $Pd^{2+}$, and the number of chloride ions involved in the coordination between cyclam and $Pd^{2+}$, we constructed ten complexes, as seen in Figure S29. Except for the non-convergent complexes, we were able to produce the stable adsorption structures after geometric optimizations. The thermodynamic viability of these stable complexes was determined by calculating their respective Gibbs free energy changes ΔG. The calculated negative ΔG values for complexes 1 (−0.12 kcal/mol), 2 (−7.07 kcal/mol), 7 (−9.14 kcal/mol), and 8 (−1.80 kcal/mol) indicate that adopting these adsorption patterns are energetically favorable for $Pd^{2+}$ adsorption. Moreover, complex 7 has the highest ΔG value, indicating that the simultaneous coordination of two $Pd^{2+}$ ions on one macrocycle, each with two N donors and two chloride ions, is the optimal adsorption pattern. The front and local views of the optimized structures of complexes 2 and 7, and the corresponding bond lengths of Pd–N in

these complexes are shown in Figure 4A. It can be seen that the $Pd^{2+}$ cations tend to adopt a planar tetra-coordinated bonding mode with the N and Cl atoms. The bond lengths of Pd–N or Pd–Cl in these complexes are all within 2.3 Å, close to those in crystal structures of Pd complexes. According to the coordination mode of complex 7, the predicted uptake for chemisorption would be 236 mg $g^{-1}$, which matches the Pd adsorption curve (Figure 3A, sharp increase from 0 to ~200 mg $g^{-1}$) very well. Then, the gradual slope could result from electrostatic interactions between $[PdCl_4]^{2-}$ and cationic Zr [Zr-OH] sites or defect sites in the framework.[59] For MOF-525 (PCN-221), the uptake mainly comes from interactions on the $Zr_6$ cluster and physical interactions with the pore surface.[59,60] Due to the aggregation and unfavorable conformation, **compound 3**'s active regions are blocked, which lead to the negligible uptake of Pd.

The flexibility of spatial arrangement and the matching softness can create a dynamic space that is responsive to specific guests.[37,61,62] This prompted us to analyze the conformation of cyclam macrocycle in MMCF-6 and its contributions to the $Pd^{2+}$ adsorption behavior of MMCF-6. A comparison of MMCF-6 and Pd@MMCF-6 indicates the distance change of two amine-N atoms from 3.22 to 2.98 Å after adsorption, which confirms the self-adaption of $Pd^{2+}$ within the cyclam macrocycle (Figure 4B). With the large ΔG values in complex 2 and 7, it implies the vital role of adaptive-adsorption for $Pd^{2+}$ capture. The decreased Gibbs free energy change (Figure S30, ΔG2* = −0.39 kcal/mol) in fixed fragments further confirms the above conclusion. The large difference suggests that this local rearrangement is energetically favored for the cavity to accommodate $Pd^{2+}$.

To gain more experimental insights into the local environment of the $Pd^{2+}$ sites in $Pd^{2+}$@MMCF-6, we measured the EXAFS to get in-depth into the electronic structure and geometric structure of Pd sites (Figure S31). The EXAFS data were modeled using the DFT-optimized $Pd^{2+}$-adsorbed fragments. For the structure provides the best EXAFS fitting with the experimental data, the adsorbing $Pd^{2+}$ is surrounded by two N atoms and two Cl (see Figure 4C; Table S11), revealing the main Pd–N bond distance $R_{Pd–N}$ = 2.10 Å and $R_{Pd–Cl}$ = 2.32 Å. Several C atoms were observed at the longer distance, including 2.74, 3.07, and 3.28 Å. These locations also match the aforementioned DFT results. The presence of Pd–Pd bonds was unobservable in the fitting. The viability of the proposed structures is illustrated by the fact that DFT calculations and EXAFS results align well with one another.

Utilizing X-ray photoelectron spectroscopy (XPS), the binding of Pd to the cyclam cavity was analyzed. The Pd 3d spectra for Pd@MMCF-6 was acquired to validate the adsorption mechanism. Two distinct peaks were seen at 343.6 and 338.4 eV, which corresponded to $3d_{3/2}$ and $3d_{5/2}$, respectively. Comparing this with the pristine MMCF-6 sample, which lacked discernible Pd 3d peaks, suggests that no Pd was left over after the ligand synthesis process (Figure S13). When compared with the as-prepared MMCF-6, the N 1s spectra of the Pd@MMCF-6 revealed a shift in the peak position toward a higher binding energy, suggesting a reduction in the electron density of N atoms due to the strong coordination of N with $Pd^{2+}$. These findings are consistent with the reported results on the coordination of $Pd^{2+}$ ions with N atoms.[63,64] MMCF-6 was also characterized by energy-dispersive X-ray spectroscopy (EDS) mapping before and after $Pd^{2+}$ adsorption. According to the EDS mapping results (Figure S12), the uniform distribution of the element Pd suggests its homogeneous adsorption on MMCF-6.

To examine the relationship between $Pd^{2+}$ capture behaviors and global structural variation, periodic dispersion-corrected DFT calculations were undertaken on MMCF-6 and Pd@MMCF-6. Based on the local atomic structure model of Pd from EXAFS experiment, Pd@MMCF-6 was built with $Pd^{2+}$ coordinating in the cyclam cavities of MMCF-6 via a tetra-topic manner with two amine-N and two chlorines, and the structure of both MMCF-6 and Pd@MMCF-6 were optimized by DFT calculations allowing all atom positions and unit cell parameters to vary. Based on the DFT simulation results of the fully relaxed models, MMCF-6 shows a *trans*-conformation for the ligand, whereas the four carboxy-phenyl groups are nearly coplanar. A minor difference of lattice parameters for these two models were observed, with 8% in lattice volume. This is reasonable to appear in the MMCF-6 system considering the flexibility brought by the cyclam macrocycles. This result corresponds quite well to the PXRD data collected following Pd capture studies (Figures S7 and S27). The unique adsorption behavior is likely the result of a mix of global and local flexibility, with the latter being the predominant contributor in the case of MMCF-6.

To enhance our understanding of the structure-Pd-recovery performance relationship, an analysis of the electrostatic potential (ESP) distribution was conducted for $H_4L$. As depicted in Figure 5A, the ESP distribution in $H_4L$ is relatively uniform. Notably, the direct linkage of N sites to the benzene ring leads to a delocalization of the N's lone pair electrons, unlike in structures with methylbenzyl groups. This delocalization appears to be a crucial factor in the high selectivity toward Pd. The highest occupied molecular orbital (HOMO) and lowest unoccupied molecular orbital (LUMO) levels of a sorbent material are critical in determining its electronic properties and its interaction with other species. The HOMO governs the electron donation ability of a molecule, whereas LUMO dictates its electron acceptance ability. The Figure 5B reveals the distribution of HOMO-LUMO within $H_4L$, the gap between HOMO-LUMO of $H_4L$ is 4.09 eV. Further insights into intermolecular and intramolecular interactions are obtained through natural bond orbital (NBO) analysis.[65–67] This analysis is instrumental in uncovering details about charge transfer and hyper-conjugative interactions, providing valuable insights for future research. A NBO analysis was conducted on the compound Pd(**L**)$Cl_2$ to investigate the degree of coordination between the N sites and Pd. This study employed a second-order perturbative NBO analysis to evaluate the Pd–N interactions within Pd(**L**)$Cl_2$. Figure 5C presents the selected set of NBOs. The analysis identified two distinct types of Pd–N interactions. The first involves a lone pair (LP) on N engaging in three interactions: LP (N) → BD*(Pd–Cl), LP (N) → LP*(Pd), and BD (C–N) → LP* (Pd). In these interactions, the N atom and the C–N bond act as donors toward the Pd–Cl bond and the Pd atom. The second type of interaction comprises LP* (Pd) → BD* (C–N), LP* (Pd) → RY*(N), and BD* (Pd–Cl) → RY*(N), where the roles of donor and acceptor are reversed. These interactions were quantified by their stabilization energies ($E^{(2)}$), with higher values indicating stronger interactions. The $E^{(2)}$ values for LP (N) → BD*(Pd–Cl), LP (N) → LP*(Pd), and BD (C–N) → LP* (Pd) were found to be 25.90, 18.65, and 9.70 kJ $mol^{-1}$, respectively. For LP* (Pd) → BD* (C–N), LP* (Pd) → RY*(N), and BD* (Pd–Cl) → RY*(N), the values were 1.45, 3.63, and 2.13 kJ $mol^{-1}$, respectively. The relatively lower stabilization energy of the second component suggests its lesser contribution to the bonding. Overall, this NBO analysis highlights that the primary interactions in Pd(**L**)$Cl_2$ are between the N sites of the ligand and the Pd. The results emphasize the pivotal role of the N sites in stabilizing the Pd adducts through strong Pd–N interactions. These interactions not only influence the overall geometry of the compound but also have significant implications for its electronic characteristics.

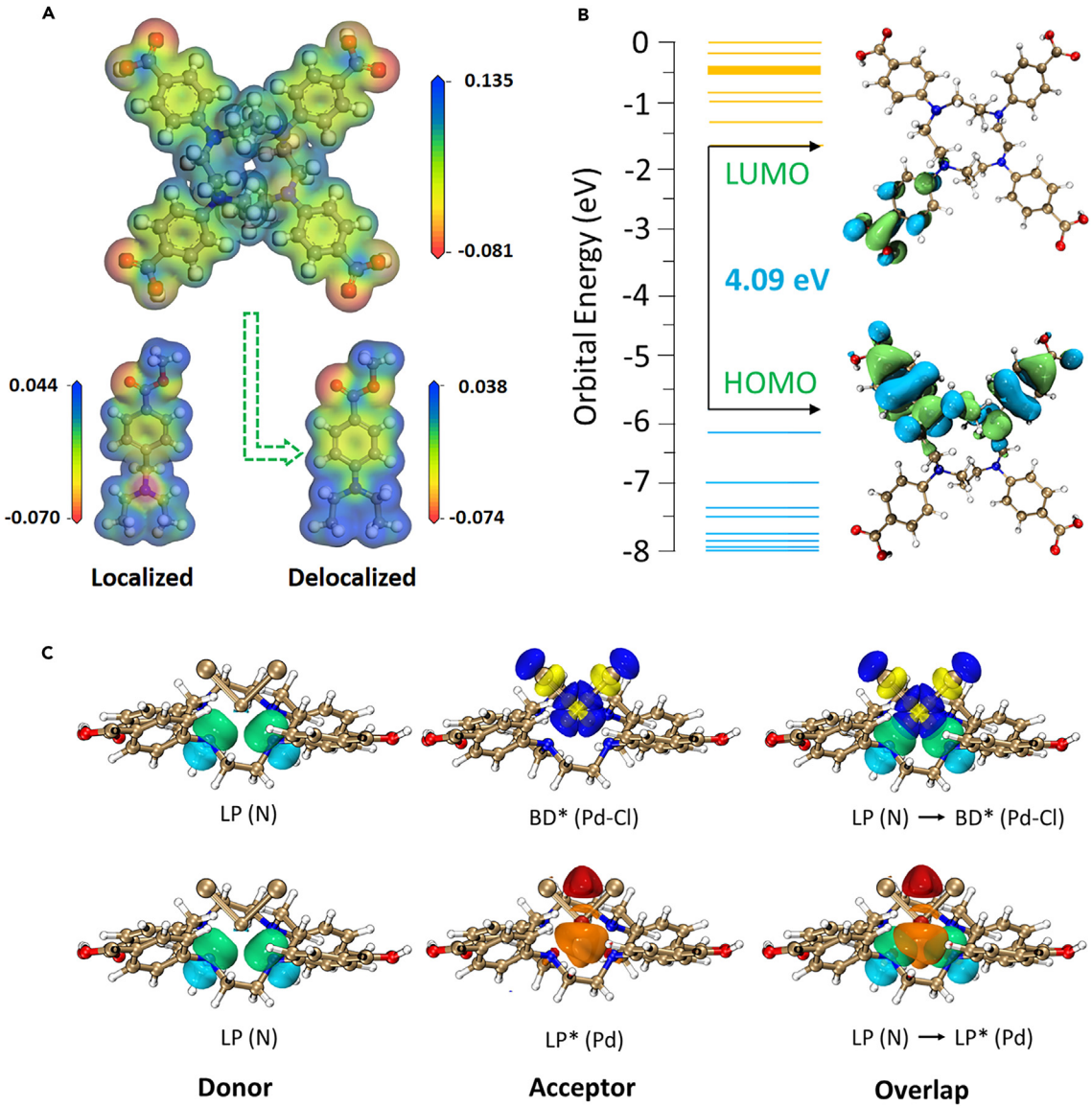


**Figure 5. DFT studies**

(A) The electrostatic potential (ESP) distribution of $H_4L$.

(B) HOMO, LUMO, and energy gap ($E_g$) for $H_4L$.

(C) Natural bond orbital (NBO) second-order perturbation theory output for "$E^{(2)}$" donor-acceptor interactions of Pd(L)$Cl_2$, showing dominant stabilization due to LP (N) → BD* (Pd–Cl) and LP (N) → LP* (Pd) delocalization, as pictured in projected NBO overlap diagrams.

Combining the above studies, it shows that the coordination effect can overwhelm the intrinsic propensities of the macrocycles in MMCF-6 for particular conformations, and we thus deduce that the $[PdCl_4]^{2-}$ was captured by the macrocycles via a coordination-driven "adaptive host-guest chemistry." In a kinetic sense, the $Pd^{2+}$ capture involves a conformation shift, that is, the migration of the N's relative positions within the cyclam macrocycle, whose binding shape is thus regarded to be complementary to the incoming guests. Evolution has produced a large array of proteins with channel and cavity architectures that can interact with substrates via dynamic motions and exact ensembles of functional groups, but this is rarely observed in synthetic molecules.[1–5] This study demonstrates

that including guest-responsive cavities in the MOF skeleton via semi-rigid macrocyclic ligands is a promising strategy for facile achieving of proteomimetic properties.

### Conclusions

We have reported a modulated synthetic approach for the construction of a novel Zr-MOF, MMCF-6, featuring accessible cyclam cavities on the basis of a rationally designed cyclam ligand with robust flexibility. The embedment of guest-responsive cavities in the MOF skeleton combined with the soft Lewis-base sites afford MMCF-6 with exceptional and precise recognition of $Pd^{2+}$. MMCF-6 demonstrates a high Pd extraction capacity of 326 mg $g^{-1}$ and an extraordinary Pd-recovery efficiency of >99.99% in aqueous solutions. The affinity between the soft Lewis acid and base induces the relocation of N donors in the cyclam macrocycle, to optimize the host-guest interactions and boost the selectivity and uptake capability for $Pd^{2+}$, which was confirmed via combined studies of X-ray crystallography, EXAFS, and DFT calculations. This strategy represents a generic practice to incorporate semi-rigid cavities into framework materials for efficient host-guest chemistry, in which rational design of the conformation of a flexible organic linker offers a route to modifying the pore geometry and internal surface chemistry and thus the function of open-framework materials.

## EXPERIMENTAL PROCEDURES

### Resource availability

#### *Lead contact*

Further information and requests for resources should be directed to and will be fulfilled by the lead contact, Shengqian Ma (shengqian.ma@unt.edu).

#### *Materials availability*

None of the unique materials generated in this study are readily available.

#### *Data and code availability*

Crystallography data for the material both from SCXRD and PXRD have been deposited at the Cambridge Crystallographic Data Centre (CCDC) under the database identifier CCDC: 2307922, CCDC: 2240667 (MMCF-6), and CCDC: 2240615 (tbtatb: tetra-tert-butyl 4,4′,4′′,4′′′-(1,4,8,11-tetraazacyclotetradecane-1,4,8,11-tetrayl)tetrabenzoate) are publicly available as of the date of publication.

## SUPPLEMENTAL INFORMATION

Supplemental information can be found online at https://doi.org/10.1016/j.chempr.2024.04.016.

## ACKNOWLEDGMENTS

This work was supported by the Robert A. Welch Foundation (B-0027). We also acknowledge the use of Advanced Photon Source, an Office of Science User Facility operated for the US Department of Energy (DOE) Office of Science by Argonne National Laboratory and that was supported by the US DOE under contract no. DE-AC02-06CH11357, and the Canadian Light Source and its funding partners. Partial support from the Researchers Supporting Project number (RSP2024R55) at King Saud University, Riyadh, Saudi Arabia, the Natural Science Foundation of Shandong Province, China (no. ZR2019MB043 and no. ZR2023MB033), and the National Natural Science Foundation of China (no. 22301039) is acknowledged as well.

## AUTHOR CONTRIBUTIONS

J.R. prepared and characterized MMCF-6. Y.Y. provided suggestions on the cryptography analysis. Y.Z. analyzed the SEM data. W.Z., J.L., and X.G. conducted the EXAF experiments and analyses. Q.L. provided suggestions on the DFT calculations. X.H. analyzed the XPS data. A.M.A.-E. and A.N. helped revise the manuscript. S.M. conceived the research.

## DECLARATION OF INTERESTS

The authors declare no competing interests.

Received: January 17, 2024
Revised: March 30, 2024
Accepted: April 23, 2024
Published: May 14, 2024

## REFERENCES

1. Zhou, L., Bosscher, M., Zhang, C., Ozçubukçu, S., Zhang, L., Zhang, W., Li, C.J., Liu, J., Jensen, M.P., Lai, L., et al. (2014). A protein engineered to bind uranyl selectively and with femtomolar affinity. Nat. Chem. *6*, 236–241. https://doi.org/10.1038/nchem.1856.

2. Swain, J.F., and Gierasch, L.M. (2006). The changing landscape of protein allostery. Curr. Opin. Struct. Biol. *16*, 102–108. https://doi.org/10.1016/j.sbi.2006.01.003.

3. Beck, D.A.C., Alonso, D.O.V., Inoyama, D., and Daggett, V. (2008). The intrinsic conformational propensities of the 20 naturally occurring amino acids and reflection of these propensities in proteins. Proc. Natl. Acad. Sci. USA *105*, 12259–12264. https://doi.org/10.1073/pnas.0706527105.

4. Katsoulidis, A.P., Antypov, D., Whitehead, G.F.S., Carrington, E.J., Adams, D.J., Berry, N.G., Darling, G.R., Dyer, M.S., and Rosseinsky, M.J. (2019). Chemical control of structure and guest uptake by a conformationally mobile porous material. Nature *565*, 213–217. https://doi.org/10.1038/s41586-018-0820-9.

5. Yang, L.P., Zhang, L., Quan, M., Ward, J.S., Ma, Y.L., Zhou, H., Rissanen, K., and Jiang, W. (2020). A supramolecular system that strictly follows the binding mechanism of conformational selection. Nat. Commun. *11*, 2740. https://doi.org/10.1038/s41467-020-16534-9.

6. Kreft, H., and Jetz, W. (2007). Global patterns and determinants of vascular plant diversity. Proc. Natl. Acad. Sci. USA *104*, 5925–5930. https://doi.org/10.1073/pnas.0608361104.

7. Zhang, S., Ding, Y., Liu, B., and Chang, C.C. (2017). Supply and demand of some critical metals and present status of their recycling in WEEE. Waste Manag. *65*, 113–127. https://doi.org/10.1016/j.wasman.2017.04.003.

8. Kang, H.-Y., and Schoenung, J.M. (2005). Electronic waste recycling: A review of U.S. infrastructure and technology options. Resour. Conserv. Recycl. *45*, 368–400. https://doi.org/10.1016/j.resconrec.2005.06.001.

9. Tanskanen, P. (2013). Management and recycling of electronic waste. Acta Mater. *61*, 1001–1011. https://doi.org/10.1016/j.actamat.2012.11.005.

10. Robinson, B.H. (2009). E-waste: an assessment of global production and environmental impacts. Sci. Total Environ. *408*, 183–191. https://doi.org/10.1016/j.scitotenv.2009.09.044.

11. Ma, Y., Zeng, J., Zeng, Y., Zhou, H., Liu, G., Liu, Y., Zeng, L., Jian, J., and Yuan, Z. (2020). Preparation and performance of poly(4-vinylpyridine)-b-polysulfone-b-poly(4-vinylpyridine) triblock copolymer/polysulfone blend membrane for separation of palladium (II) from electroplating wastewaters. J. Hazard. Mater. *384*, 121277. https://doi.org/10.1016/j.jhazmat.2019.121277.

12. Alyapyshev, M.Y., Babain, V.A., Tkachenko, L.I., Eliseev, I.I., Didenko, A.V., and Petrov, M.L. (2011). Dependence of Extraction Properties of 2,6-Dicarboxypyridine Diamides on Extractant Structure. Solvent Extr. Ion Exch. *29*, 619–636. https://doi.org/10.1080/07366299.2011.581049.

13. Ruhela, R., Singh, A.K., Tomar, B.S., and Hubli, R.C. (2014). Separation of palladium from high level liquid waste – A review. RSC Adv. *4*, 24344–24350. https://doi.org/10.1039/c4ra02024c.

14. Bianchi, A., Micheloni, M., and Paoletti, P. (1991). Thermodynamic aspects of the polyazacycloalkane complexes with cations and anions. Coord. Chem. Rev. *110*, 17–113. https://doi.org/10.1016/0010-8545(91)80023-7.

15. Wu, F., Ye, G., Yi, R., Sun, T., Xu, C., and Chen, J. (2016). Novel polyazamacrocyclic receptor decorated core–shell superparamagnetic microspheres for selective binding and magnetic enrichment of palladium: synthesis, adsorptive behavior and coordination mechanism. Dalton Trans. *45*, 9553–9564. https://doi.org/10.1039/c6dt01024e.

16. Stolzenberg, A.M., and Schussel, L.J. (1991). Synthesis, Characterization, and Electrochemistry of Copper(II) and Pailadium(II) Hydroporphyrins: The Copper(I) Octaethylisobacteriochlorin Anion. Inorg. Chem. *30*, 3205–3213. https://doi.org/10.1021/ic00016a019.

17. Wu, F., Ye, G., Liu, Y., Yi, R., Huo, X., Lu, Y., and Chen, J. (2016). New short-channel SBA-15 mesoporous silicas functionalized with polyazamacrocyclic ligands for selective capturing of palladium ions in $HNO_3$ media. RSC Adv. *6*, 66537–66547. https://doi.org/10.1039/c6ra11778c.

18. Wu, F., Yang, C., Liu, Y., Hu, S., Ye, G., and Chen, J. (2020). Novel polyazamacrocyclic receptor impregnated macroporous polymeric resins for highly efficient capture of palladium from nitric acid media. Sep. Purif. Technol. *233*, 115953. https://doi.org/10.1016/j.seppur.2019.115953.

19. Suh, M.P., and Moon, H.R. (2006). Coordination Polymer Open Frameworks Constructed of Macrocyclic Complexes. Adv. Inorg. Chem. *59*, 39–79. https://doi.org/10.1016/s0898-8838(06)59002-6.

20. Lim, D.W., Chyun, S.A., and Suh, M.P. (2014). Hydrogen storage in a potassium-ion-bound metal-organic framework incorporating crown ether struts as specific cation binding sites. Angew. Chem. Int. Ed. Engl. *53*, 7819–7822. https://doi.org/10.1002/anie.201404265.

21. Li, J., Yim, D., Jang, W.D., and Yoon, J. (2017). Recent progress in the design and applications of fluorescence probes containing crown ethers. Chem. Soc. Rev. *46*, 2437–2458. https://doi.org/10.1039/c6cs00619a.

22. Zheng, B., Wang, F., Dong, S., and Huang, F. (2012). Supramolecular polymers constructed by crown ether-based molecular recognition. Chem. Soc. Rev. *41*, 1621–1636. https://doi.org/10.1039/c1cs15220c.

23. An, S., Xu, Q., Ni, Z., Hu, J., Peng, C., Zhai, L., Guo, Y., and Liu, H. (2021). Construction of Covalent Organic Frameworks with Crown Ether Struts. Angew. Chem. Int. Ed. Engl. *60*, 9959–9963. https://doi.org/10.1002/anie.202101163.

24. Pearson, R.G. (1963). Hard and soft acids and bases. J. Am. Chem. Soc. *85*, 3533–3539. https://doi.org/10.1021/ja00905a001.

25. Liang, X., and Sadler, P.J. (2004). Cyclam complexes and their applications in medicine.

Chem. Soc. Rev. *33*, 246–266. https://doi.org/10.1039/b313659k.

26. Jermakowicz-Bartkowiak, D. (2007). A preliminary evaluation on the use of the cyclam functionalized resin for the noble metals sorption. React. Funct. Polym. *67*, 1505–1514. https://doi.org/10.1016/j.reactfunctpolym.2007.07.032.

27. Kavaklı, C., Özvatan, N., Tuncel, S.A., and Salih, B. (2002). 1,4,8,11-Tetraazacyclotetradecane bound to poly(p-chloromethylstyrene–ethylene glycol dimethacrylate) microbeads for selective gold uptake. Anal. Chim. Acta *464*, 313–322. https://doi.org/10.1016/S0003-2670(02)00484-1.

28. Elias, H. (1999). Kinetics and mechanism of metal complex formation with $N_4$-donor macrocycles of the cyclam type. Coord. Chem. Rev. *187*, 37–73. https://doi.org/10.1016/S0010-8545(98)00227-6.

29. Meyer, M., Dahaoui-Gindrey, V., Lecomte, C., and Guilard, R. (1998). Conformations and coordination schemes of carboxylate and carbamoyl derivatives of the tetraazamacrocycles cyclen and cyclam, and the relation to their protonation states. Coord. Chem. Rev. *178–180*, 1313–1405. https://doi.org/10.1016/S0010-8545(98)00169-6.

30. McAuley, A., and Subramanian, S. (2000). Formation of multinuclear complexes: new developments from cyclam derivatives. Coord. Chem. Rev. *200–202*, 75–103. https://doi.org/10.1016/S0010-8545(00)00341-6.

31. Lee, E.Y., and Suh, M.P. (2004). A Robust Porous Material Constructed of Linear Coordination Polymer Chains: Reversible Single-Crystal to Single-Crystal Transformations upon Dehydration and Rehydration. Angew. Chem. Int. Ed. Engl. *43*, 2798–2801. https://doi.org/10.1002/ange.200353494.

32. Suh, M.P., Moon, H.R., Lee, E.Y., and Jang, S.Y. (2006). A Redox-Active Two-Dimensional Coordination Polymer: Preparation of Silver and Gold Nanoparticles and Crystal Dynamics on Guest Removal. J. Am. Chem. Soc. *128*, 4710–4718. https://doi.org/10.1021/ja056963l.

33. Zhu, X., Lü, J., Li, X., Gao, S., Li, G., Xiao, F., and Cao, R. (2008). Syntheses, structures, near-infrared, and visible luminescence of lanthanide-organic frameworks with flexible macrocyclic polyamine ligands. Cryst. Growth Des. *8*, 1897–1901. https://doi.org/10.1021/cg701098t.

34. Furukawa, H., Cordova, K.E., O'Keeffe, M., and Yaghi, O.M. (2013). The chemistry and applications of metal-organic frameworks. Science *341*, 1230444. https://doi.org/10.1126/science.1230444.

35. Zhou, H.C.J., and Kitagawa, S. (2014). Metal-organic frameworks (MOFs). Chem. Soc. Rev. *43*, 5415–5418. https://doi.org/10.1039/c4cs90059f.

36. Zhou, H.C., Long, J.R., and Yaghi, O.M. (2012). Introduction to metal-organic frameworks. Chem. Rev. *112*, 673–674. https://doi.org/10.1021/cr300014x.

37. Zeng, H., Xie, M., Wang, T., Wei, R.J., Xie, X.J., Zhao, Y., Lu, W., and Li, D. (2021). Orthogonal-array dynamic molecular sieving of propylene/propane mixtures. Nature *595*, 542–548. https://doi.org/10.1038/s41586-021-03627-8.

38. Martí-Gastaldo, C., Antypov, D., Warren, J.E., Briggs, M.E., Chater, P.A., Wiper, P.V., Miller, G.J., Khimyak, Y.Z., Darling, G.R., Berry, N.G., et al. (2014). Side-chain control of porosity closure in single- and multiple-peptide-based porous materials by cooperative folding. Nat. Chem. *6*, 343–351. https://doi.org/10.1038/nchem.1871.

39. Zhang, H., Zou, R., and Zhao, Y. (2015). Macrocycle-based metal-organic frameworks. Coord. Chem. Rev. *292*, 74–90. https://doi.org/10.1016/j.ccr.2015.02.012.

40. Roy, I., and Stoddart, J.F. (2021). Cyclodextrin Metal-Organic Frameworks and Their Applications. Acc. Chem. Res. *54*, 1440–1453. https://doi.org/10.1021/acs.accounts.0c00695.

41. Huang, N.Y., Zhang, X.W., Xu, Y.Z., Liao, P.Q., and Chen, X.M. (2019). A local hydrophobic environment in a metal-organic framework for boosting photocatalytic CO2 reduction in the presence of water. Chem. Commun. (Camb) *55*, 14781–14784. https://doi.org/10.1039/c9cc08094e.

42. Gong, W., Xie, Y., Wang, X., Kirlikovali, K.O., Idrees, K.B., Sha, F., Xie, H., Liu, Y., Chen, B., Cui, Y., et al. (2023). Programmed Polarizability Engineering in a Cyclen-Based Cubic Zr(IV) Metal-Organic Framework to Boost Xe/Kr Separation. J. Am. Chem. Soc. *145*, 2679–2689. https://doi.org/10.1021/jacs.2c13171.

43. Zhu, J., Usov, P.M., Xu, W., Celis-Salazar, P.J., Lin, S., Kessinger, M.C., Landaverde-Alvarado, C., Cai, M., May, A.M., Slebodnick, C., et al. (2018). A New Class of Metal-Cyclam-Based Zirconium Metal–Organic Frameworks for CO2 Adsorption and Chemical Fixation. J. Am. Chem. Soc. *140*, 993–1003. https://doi.org/10.1021/jacs.7b10643.

44. Zhu, X.-D., Tao, T.-X., Zhou, W.-X., Wang, F.-H., Liu, R.-M., Liu, L., and Fu, Y.-Q. (2014). A novel lead(II) porous metal–organic framework constructed from a flexible bifunctional macrocyclic polyamine ligand. Inorg. Chem. Commun. *40*, 116–119. https://doi.org/10.1016/j.inoche.2013.11.042.

45. Stackhouse, C.A., and Ma, S. (2018). Azamacrocyclic-based metal organic frameworks: Design strategies and applications. Polyhedron *145*, 154–165. https://doi.org/10.1016/j.poly.2018.01.036.

46. Zhu, X.-D., Lin, Z.-J., Liu, T.-F., Xu, B., and Cao, R. (2012). Two Novel 3d-4f Heterometallic Frameworks Assembled from a Flexible Bifunctional Macrocyclic Ligand. Cryst. Growth Des. *12*, 4708–4711. https://doi.org/10.1021/cg300848f.

47. Dorel, R., Grugel, C.P., and Haydl, A.M. (2019). The Buchwald-Hartwig Amination After 25 Years. Angew. Chem. Int. Ed. Engl. *58*, 17118–17129. https://doi.org/10.1002/anie.201904795.

48. Reichelt, A., Falsey, J.R., Rzasa, R.M., Thiel, O.R., Achmatowicz, M.M., Larsen, R.D., and Zhang, D. (2010). Palladium-Catalyzed Chemoselective Monoarylation of Hydrazides for the Synthesis of[1,2,4]Triazolo[4,3-a]pyridines. Org. Lett. *12*, 792–795. https://doi.org/10.1021/ol902868q.

49. Nakanishi, M., and Bolm, C. (2006). Palladium-Catalyzed N-Arylations of 1,4,7-Triazacyclononanes. Adv. Synth. Catal. *348*, 1823–1825. https://doi.org/10.1002/adsc.200606196.

50. Ruiz-Castillo, P., and Buchwald, S.L. (2016). Applications of Palladium-Catalyzed C-N Cross-Coupling Reactions. Chem. Rev. *116*, 12564–12649. https://doi.org/10.1021/acs.chemrev.6b00512.

51. Ravikovitch, P.I., and Neimark, A.V. (2002). Experimental Confirmation of Different Mechanisms of Evaporation from Ink-Bottle Type Pores: Equilibrium, Pore Blocking, and Cavitation. Langmuir *18*, 9830–9837. https://doi.org/10.1021/la026140z.

52. Bourgeois, D., Lacanau, V., Mastretta, R., Contino-Pépin, C., and Meyer, D. (2020). A simple process for the recovery of palladium from wastes of printed circuit boards. Hydrometallurgy *191*, 105241. https://doi.org/10.1016/j.hydromet.2019.105241.

53. Liu, H., Ning, S., Zhang, S., Wang, X., Chen, L., Fujita, T., and Wei, Y. (2022). Preparation of a mesoporous ion-exchange resin for efficient separation of palladium from simulated electroplating wastewater. J. Environ. Chem. Eng. *10*, 106966. https://doi.org/10.1016/j.jece.2021.106966.

54. Firmansyah, M.L., Kubota, F., and Goto, M. (2019). Selective Recovery of Platinum Group Metals from Spent Automotive Catalysts by Leaching and Solvent Extraction. J. Chem. Eng. Jpn. *52*, 835–842. https://doi.org/10.1252/jcej.19we093.

55. Bai, Y., Chen, L., He, L., Li, B., Chen, L., Wu, F., Chen, L., Zhang, M., Liu, Z., Chai, Z., et al. (2022). Precise recognition of palladium through interlaminar chelation in a covalent organic framework. Chem *8*, 1442–1459. https://doi.org/10.1016/j.chempr.2022.02.016.

56. Pearson, R.G. (1968). Hard and soft acids and bases HSAB part 1: fundamental-principles. J. Chem. Educ. *45*, 581–587. https://doi.org/10.1021/ed045p581.

57. Hamisu, A.M., Ariffin, A., and Wibowo, A.C. (2020). Cation exchange in metal-organic frameworks (MOFs): The hard-soft acid-base (HSAB) principle appraisal. Inorg. Chim. Acta *511*. https://doi.org/10.1016/j.ica.2020.119801.

58. Pearson, R.G. (2005). Chemical hardness and density functional theory. J. Chem. Sci. *117*, 369–377. https://doi.org/10.1007/bf02708340.

59. Lin, S., Zhao, Y., Bediako, J.K., Cho, C.-W., Sarkar, A.K., Lim, C.-R., and Yun, Y.-S. (2019). Structure-controlled recovery of palladium(II) from acidic aqueous solution using metal-organic frameworks of MOF-802, UiO-66 and MOF-808. Chem. Eng. J. *362*, 280–286. https://doi.org/10.1016/j.cej.2019.01.044.

60. Lin, S., Kumar Reddy, D.H., Bediako, J.K., Song, M.-H., Wei, W., Kim, J.-A., and Yun, Y.-S. (2017). Effective adsorption of Pd(II), Pt(IV) and Au(III) by Zr(IV)-based metal–organic frameworks from strongly acidic solutions. J. Mater. Chem. A *5*, 13557–13564. https://doi.org/10.1039/c7ta02518a.

61. Niu, Z., Fan, Z., Pham, T., Verma, G., Forrest, K.A., Space, B., Thallapally, P.K., Al-Enizi, A.M., and Ma, S. (2022). Self-Adjusting Metal-Organic Framework for Efficient Capture of Trace Xenon and Krypton. Angew. Chem. Int. Ed. Engl. *61*, e202117807. https://doi.org/10.1002/anie.202117807.

62. Tian, J., Chen, Q., Jiang, F., Yuan, D., and Hong, M. (2023). Optimizing Acetylene Sorption through Induced-fit Transformations in a Chemically Stable Microporous Framework. Angew. Chem. Int. Ed. Engl. *62*, e202215253. https://doi.org/10.1002/anie.202215253.

63. Drelinkiewicz, A., Hasik, M., and Choczyński, M. (1998). Preparation and properties of polyaniline containing palladium. Mater. Res. Bull. *33*, 739–762. https://doi.org/10.1016/S0025-5408(98)00042-7.

64. Kang, E.T., Neoh, K.G., and Tan, K.L. (1990). XPS studies of charge-transfer interactions in some pyridine: organic-acceptor complexes. Mol. Phys. *70*, 1057–1064. https://doi.org/10.1080/00268979000101521.

65. Humphrey, W., Dalke, A., and Schulten, K. (1996). VMD: Visual Molecular Dynamics. J. Mol. Graph. *14*, 33–38. https://doi.org/10.1016/0263-7855(96)00018-5.

66. Lu, T., and Chen, F. (2012). Multiwfn: a multifunctional wavefunction analyzer. J. Comput. Chem. *33*, 580–592. https://doi.org/10.1002/jcc.22885.

67. Foster, J.P., and Weinhold, F. (1980). Natural Hybrid Orbitals. J. Am. Chem. Soc. *102*, 7211–7218. https://doi.org/10.1021/ja00544a007.